THIS MONTH IN

JNM

Hachamovitch and Di Carli assess past evidence and new findings on the potential role of automatic quantitative software in the interpretation and reporting of results of stress myocardial perfusion scintigraphy. . . . . ***Page 194***

Van der Wall and colleagues survey sometimes-contentious current viewpoints on the use of radioguided minimally invasive surgery for localization of parathyroid adenoma. . ***Page 198***

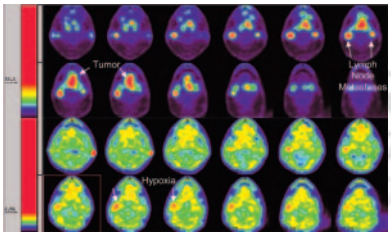

Boersma and colleagues discuss the background and controversies surrounding cell transplantation technologies and provide additional context for the article in this issue on radiotracing neural stem cells by Kim and colleagues. . . . . ***Page 200***

Leslie and colleagues report on the quality of prognostic information provided by automated quantification of ^{99m}Tc-sestamibi SPECT myocardial perfusion scans and the ability of this technique to complement conventional visual image interpretation. . . . . ***Page 204***

Jagathesan and colleagues describe the use of $H_2{}^{15}O$ PET in a reproducible technique for the determination of myocardial blood flow and coronary reserve after pharmacologic stress in patients with stable coronary artery disease. . ***Page 212***

Rubello and colleagues report the results of a multicenter study on the diagnostic accuracy of ^{99m}Tc-sestamibi scintigraphy and neck ultrasonography in primary hyperparathyroidism and on the value of intraoperative hand-held γ-probes in minimally invasive radioguided surgery for solitary parathyroid adenoma. . ***Page 220***

Weintraub and colleagues correlate the results of ^{99m}Tc-TRODAT-1 SPECT imaging of striatal dopamine transporters with symptoms of anxiety and depression in patients with Parkinson's disease. . . . . ***Page 227***

Jeong and colleagues employ voxelwise analysis of ^{18}F-FDG PET images of patients with frontotemporal dementia to identify distinctive areas of hypometabolism that may provide keys to differentiating this degenerative process from other dementias. . . . . ***Page 233***

Gallezot and colleagues report on the utility of ^{18}F-fluoro-A-85380, a PET radioligand, for estimating the regional brain distribution of nicotinic acetylcholine receptors in human neurodegenerative diseases. . . . . ***Page 240***

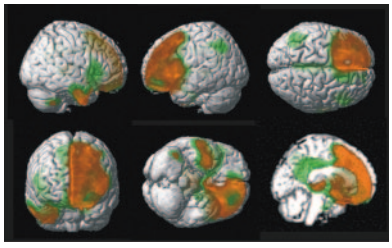

Gayed and colleagues compare the clinical values of simultaneously acquired ^{99m}Tc-sestamibi SPECT/CT and conventional SPECT in diagnosing and locating parathyroid adenomas or hyperplasia in patients with primary hyperparathyroidism. . . . . ***Page 248***

Eschmann and colleagues evaluate the kinetic behavior of the PET tracer ^{18}F-fluoromisonidazole as a predictor of tumor recurrence after radiotherapy in a group of patients with advanced non–small cell lung or head and neck cancer. . . . . ***Page 253***

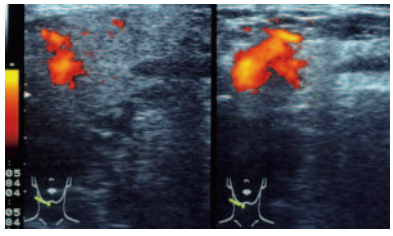

Nakada and colleagues report on the surprising results of a study to determine whether the widely used practice of sucking lemon candy early after high-dose radioiodine therapy for postsurgical differentiated thyroid cancer actually reduces salivary gland dysfunction and injury. . ***Page 261***

Higashi and colleagues examine the results of a multicenter study to determine whether ^{18}F-FDG uptake by primary tumor is a predictor of intratumoral lymphatic vessel invasion and lymph node metastasis in patients with non–small cell lung cancer. . . . . ***Page 267***

Muzi and colleagues describe the application of a model of kinetics for ^{18}F-FLT PET to facilitate in vitro and in vivo measures of cellular proliferation in tumor. . ***Page 274***

Yau and colleagues focus on the question of whether intravenous iodinated contrast agents in PET/CT introduce significant attenuation correction errors resulting in erroneous ^{18}F-FDG uptake values. . . . . ***Page 283***

Sun and colleagues examine the selective retention of the pyrimidine analog ^{18}F-FMAU in DNA in proliferating tissue and suggest this as a possible alternative to ^{11}C-thymidine for imaging DNA synthesis in normal tissues and tumors. . . . . ***Page 292***

Shoup and colleagues describe radiosynthesis and preliminary biologic evaluation of ^{18}F-FCPHA as a novel potential probe for assessing myocardial fatty acid metabolism with PET. . . . . ***Page 297***

Kim and colleagues report on a method for reversing silencing of human sodium/iodide symporter transgenes transfected in human neural stem cells and speculate on the implications of this technique for monitoring novel therapies. . . ***Page 305***

Benveniste and colleagues report on the ability of PET with MRI to assess uptake and distribution of ^{11}C-cocaine in late pregnancy in a simian model, with promising implications for directly and simultaneously measuring the accumulation of cocaine or its radiolabeled metabolites in maternal and fetal organs. . . . ***Page 312***

Kwon and colleagues assess the experimental utility of ^{99m}Tc-galactosyl-human serum albumin as a scintigraphic tracer for the assessment of hepatocytes and as a potential tool for monitoring hepatic ischemia and preventing reperfusion injury. . . . . ***Page 321***

Pomper and colleagues describe the development of an array of α_7-selective nicotinic cholinergic receptor–based imaging agents for PET and SPECT. . ***Page 326***

Celler and colleagues examine issues related to the quality of attenuation maps generated in SPECT imaging and the effects that map artifacts may have on attenuation-corrected emission images. . . . ***Page 335***

Shah and colleagues introduce a paired-image radiation transport methodology designed to provide a more realistic 3D geometry and detailed modeling for skeletal dose assessment in radionuclide therapies. . . . . ***Page 344***

Sharma and colleagues report on investigations of a tracer for molecular imaging of the functional transport activity of *MDR1* P-glycoprotein that may enable noninvasive SPECT/PET monitoring of the blood–brain barrier, chemotherapeutic regimens, and *MDR1* gene therapy protocols in vivo. . . . . ***Page 354***

Paik and colleagues investigate the stimulating effect of exogenous nitrous oxide on ^{18}F-FDG transport in human endothelial cells and point to findings that suggest an important role for nitrous oxide for modulating glucose transport on these cells. . . . . ***Page 365***

Muzi and colleagues augment their companion article in this issue with a method to measure regional rates of cellular proliferation in ^{18}F-FLT imaging and describe model behavior and expected values for the accuracy of parameter estimates for this tracer. . . . . ***Page 371***

ON THE COVER

In this paired-image radiation transport (PIRT) model for the right proximal femur of a 66-y-old man, the macrostructural model (obtained by ex vivo CT) is at top right and 3-dimensional NMR microscopy images are at bottom middle and right. For each tissue source region, 2 different transport simulations are performed—one in which electrons are started within the spongiosa of the femoral head (orange voxels) and one in which electrons are started within the spongiosa of the femoral neck (red voxels). Only the corresponding NMR microscopy image is used within the PIRT model (head or neck microimage). Final absorbed fractions for the entire proximal femur are taken as mass-weighted averages of results from the head-only and neck-only spongiosa source transport calculations.